Study of Systematic Bias in Measuring Surface Deformation with SAR Interferometry

Homa Ansari [1], Francesco De Zan [2], and Alessandro Parizzi [2]

[1]German Aerospace Center (DLR)
[2]Affiliation not available

October 30, 2023

Abstract

This paper investigates the presence of a new interferometric signal in multilooked Synthetic Aperture Radar (SAR) interferograms which cannot be attributed to atmospheric or earth surface topography changes. The observed signal is short-lived and decays with temporal baseline; however, it is distinct from the stochastic noise usually attributed to temporal decorrelation. The presence of such fading signal introduces a systematic phase component, particularly in short temporal baseline interferograms. If unattended, it biases the estimation of Earth surface deformation from SAR time series.

The contribution of the mentioned phase component is quantitatively assessed. For short temporal baseline interferograms, we quantify the phase contribution to be in the regime of 5 rad at C-band. The biasing impact on deformation signal retrieval is further evaluated. As an example, exploiting a subset of short temporal baseline interferograms which connects each acquisition with the successive 5 in the time series, a significant bias of -6.5 mm/yr is observed in the estimation of deformation velocity from a four-year Sentinel-1 data stack. A practical solution for mitigation of this physical fading signal is further discussed; special attention is paid to the efficient processing of Big Data from modern SAR missions such as Sentinel-1 and NISAR. Adopting the proposed solution, the deformation bias is shown to decrease to -0.24 mm/yr for the Sentinel-1 time series.

Based on these analyses, we put forward our recommendations for efficient and accurate deformation signal retrieval from large stacks of multilooked interferograms.

This is a pre-print version submitted to IEEE Transactions on Geoscience and Remote Sensing

Study of Systematic Bias in Measuring Surface Deformation with SAR Interferometry

Homa Ansari, Francesco De Zan, Alessandro Parizzi

***Abstract*—This paper investigates the presence of a new interferometric signal in multilooked Synthetic Aperture Radar (SAR) interferograms which cannot be attributed to atmospheric or earth surface topography changes. The observed signal is short-lived and decays with temporal baseline; however, it is distinct from the stochastic noise usually attributed to temporal decorrelation. The presence of such fading signal introduces a systematic phase component, particularly in short temporal baseline interferograms. If unattended, it biases the estimation of Earth surface deformation from SAR time series.**

The contribution of the mentioned phase component is quantitatively assessed. For short temporal baseline interferograms, we quantify the phase contribution to be in the regime of 5 rad at C-band. The biasing impact on deformation signal retrieval is further evaluated. As an example, exploiting a subset of short temporal baseline interferograms which connects each acquisition with the successive 5 in the time series, a significant bias of -6.5 mm/yr is observed in the estimation of deformation velocity from a four-year Sentinel-1 data stack. A practical solution for mitigation of this physical fading signal is further discussed; special attention is paid to the efficient processing of Big Data from modern SAR missions such as Sentinel-1 and NISAR. Adopting the proposed solution, the deformation bias is shown to decrease to -0.24 mm/yr for the Sentinel-1 time series.

Based on these analyses, we put forward our recommendations for efficient and accurate deformation signal retrieval from large stacks of multilooked interferograms.

***Index Terms*—Big Data, deformation estimation, differential interferometric synthetic aperture radar (DInSAR), distributed scatterers, error analysis, near real time processing, phase inconsistencies, signal decorrelation, time series analysis.**

I. Introduction

As an established geodetic technique for Earth surface deformation monitoring, the accuracy of the Interferometric Synthetic Aperture Radar (InSAR) time series analysis should be well quantified and the potential error sources must be known. Any uncertainty in the accuracy of InSAR products compromises their reliability in sensitive applications.

Persistent Scatterer Interferometry (PSI) is among the pioneering techniques for improving the accuracy of InSAR [1] in deformation retrieval. Exploiting the phase stable Persistent Scatterers (PS) within the time series, PSI avoids a major limitation of InSAR, namely the signal decorrelation [2]. Using the high Signal to Noise Ratio (SNR) PS measurements, another error source of InSAR is mitigated through the separation of the atmospheric signals from the deformation. PSI technique has been perfected since its invention and its accuracy has been studied thoroughly [3].

The authors are with the German Aerospace Center (DLR), Remote Sensing Technology Institute (IMF), 82234 Wessling, Germany (email: homa.ansari@dlr.de).

The low density of PS in non urban areas motivated the invention of complementary techniques to PSI. These methods exploit partially decorrelating areas in time series analysis. Referred to as Distributed Scatterers (DS), such areas pertain to an ensemble of natural scatterers which share similar scattering characteristics. A variety of methods have been put forward to allow the use of DS in deformation estimation, with Small BAseline Subset algorithm (SBAS) [4] and SqueeSAR [5] as the overarching approaches. The shortcoming of natural scatterers of DS is their inherent phase noise caused by signal decorrelation. Common to all DS techniques, spatial averaging, or multilooking, is employed to reduce this stochastic noise in the interferograms.

The purpose of this paper is to investigate the accuracy of multilooked interferograms with regards to DS techniques. Different studies have been dedicated to the validation of DS with independent geodetic techniques, such as Global Navigation Satellite Systems (GNSS) measurements (see e.g. [6]). Being spatially sparse, such independent measurements restrict the comprehensive study of the DS behavior. Here we consider a different validation approach to reveal a peculiar systematic signal in multilooked interferograms. If unattended, the mentioned signal can severely bias the deformation estimates of DS. We investigate the accuracy of deformation estimates in the presence of this signal to highlight the role of different DS techniques in either exacerbation or mitigation of deformation bias.

Following the theoretical background of section II, we design different comparison approaches in section III, to shed light on the following propositions:

- the multilooked interferograms reveal a systematic signal which cannot be explained by the topographic or atmospheric variations and interfere in the accurate estimation of the deformation. Such signals are short-lived and decay with the temporal baseline, rendering the short temporal baseline interferograms to be more error-prone. Hereafter we refer to this effect as the *fading signal* to reflect that it is inherently a short-lived but physical phase contribution;
- at interferogram level, the magnitude of the signal can be small as compared to the well-known InSAR error sources such as atmospheric perturbations. However, the propagation of this negligibly small error through the time series of interferograms compromises the accuracy of deformation;
- focusing on two conventional InSAR deformation products, the estimates of surface displacement time series and displacement velocity are both compromised in the presence of the fading signal;
- the fading signal may be induced by different physical

phenomena. The understanding of the source of this signal and its modeling is a current research topic [7], [12], [13]. Lacking a generic model to explain the behavior of fading signal makes the calibration of these errors intricate;
- using the temporal data redundancy within the time series, i.e. by exploiting all possible interferograms, the fading signal is significantly mitigated in the multilooked interferograms. This mitigation improves the accuracy of both displacement time series and displacement velocity estimates.

After the careful examination of these propositions in section IV, we put forward our suggestions for achieving accurate deformation monitoring with DS in section V.

II. Technical Background

A. Single-look versus Multilooked Observations

In a time series of n Synthetic Aperture Radar (SAR) acquisitions, each pair of a so called master and slave acquisitions allow the formation of an interferogram. The latter is the phase difference between the two complex valued images, relative to the master acquisition. For each choice of master acquisition, $n-1$ *common-master* interferograms exist within the time series. In total, $n(n-1)/2$ *multimaster* interferograms may be formed for each time series. As the target of geodetic applications, Earth surface deformation is estimated from all or a subset of these interferograms. Therefore, the accuracy of the deformation estimates is governed by the quality and the number of the exploited interferograms.

In this work, we distinguish between two types of observations in interferograms: single-look versus the multilooked interferometric phases. The former is for instance related to the PS, where the single complex valued pixels are exploited within the time series. The latter observations are the result of spatial averaging as common for DS regions.

For the case of PS, the multimaster interferograms of the single-look observations are highly redundant. A mere subset of $n-1$ common-master interferograms allows the reconstruction of all possible interferogram combinations within the time series e.g.:

$$\begin{aligned} &\text{for PS} : \Delta\phi_{ik} = \mathrm{W}(\Delta\phi_{im} - \Delta\phi_{km}) \\ &\quad \rightarrow \Delta\phi_{imk} = \mathrm{W}(\Delta\phi_{im} - \Delta\phi_{km} - \Delta\phi_{ik}) = 0. \end{aligned} \tag{1}$$

Here $\mathrm{W}(x) = \mathrm{mod}\{x+\pi, 2\pi\} - \pi$, m indexes the master acquisition and $\Delta\phi_{imk}$ is an indicator for the consistency of phase components within the time series [7].

As the second category of observations, DS are characterized by homogeneous areas which undergo signal decorrelation. Therefore the single-look observations within the DS region have low SNR. The remedy in improving the SNR is to perform spatial averaging within homogeneous DS region and form multilooked observations. All advanced DS-InSAR techniques employ multilooking, although some techniques attempt to include the high-frequency signals [8] or use data-adaptive and thereby feature-preserving methods [5], [9]. Although effective in noise reduction, multilooking changes the statistical properties of the interferograms. It reduces the redundancy among the $n(n-1)/2$ interferogram combinations, such that (1) no longer holds. A residual component is observed among each three arbitrary multilooked interferograms i.e.:

$$\text{for DS} : \Delta\phi_{imk} = \mathrm{W}(\Delta\phi_{im} + \Delta\phi_{mk} + \Delta\phi_{ki}) \neq 0; \tag{2}$$

implying that the phase information of the DS regions is *inconsistent* among arbitrary interferograms. Two effects may be observed for the DS phases:
- $\mathbb{E}\{\Delta\phi_{imk}\} = 0$ reflecting stochastic noise caused by signal decorrelation;
- $\mathbb{E}\{\Delta\phi_{imk}\} \neq 0$ indicating a variant systematic signal among the multilooked interferograms;

where $\mathbb{E}$ shows the statistical expectation of the accompanied random variable.

The former stochastic effect translates to noise in the deformation estimates. More critical is the latter systematic effect which may be present in a subset of the interferograms and therefore revealed in certain interferogram triplets. The systematic effects introduce an fading signal in the affected multilooked interferograms. If present and not mitigated properly, they are interpreted as deformation and bias the estimates.

The peculiar fading signal is raised by multilooking and absent in single-look observations. Therefore the discrepancy between the single-look and multilooked observations can be used to investigate firstly the presence of the fading signals and finally their impact on biasing the deformation estimates. This rationale is adopted throughout this paper and expanded in section III-B and III-C.

As the target for geodetic application, the atmospheric and surface deformation signals are consistent within arbitrary interferograms [7], i.e. $\Delta\phi_{imk} = 0$ holds for the phase components corresponding to these signals. The reason is that these physical sources uniformly affect all scatterers within the DS region, therefore their net residual effect vanishes in $\mathbb{E}\{\Delta\phi_{imk}\}$ [7], [10]. To safeguard against the fading signals, one needs to retrieve the consistent component of the interferograms or in other words reconstruct the consistency among them.

B. Reconstruction of consistency

One approach to reconstruct the consistency is to discover the physical source of the fading signals, accurately model their scattering behavior, and thereby phase contribution, and compensate the corresponding phase from the multilooked interferograms. As one source of the fading signals, we refer the reader to the variation in the moisture content of the scattering media. The effect of moisture on InSAR is studied and modeled in [12]. Based on the proposed moisture model, the corresponding phase contribution is estimated from the residual phase of (2) in [13]. The multilooked interferograms may further be compensated by the estimated moisture-induced phase to form consistent interferograms [13]. The consistency in this case is reconstructed via calibrating the fading signal's phase component.

As the analysis of this paper reveals, the mentioned moisture model does not suffice in explaining the observed inconsistencies (see section IV-E), rendering the calibration ineffective.

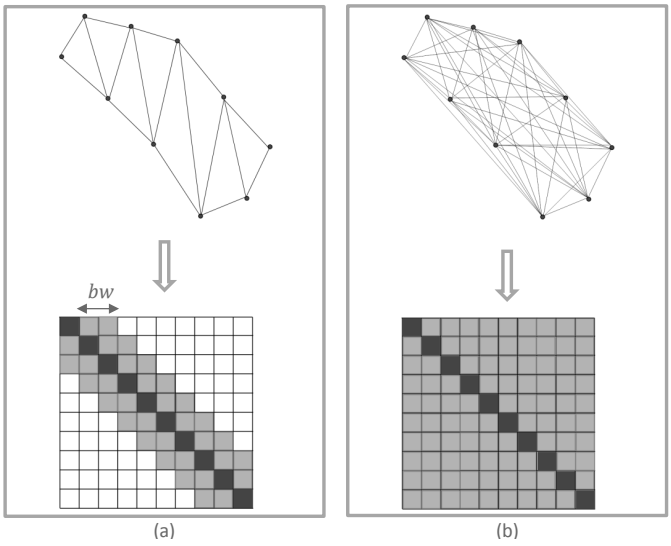

Fig. 1: Different levels of data exploitation within interferogram stacks. Top sketch mimics SAR images with dots and the exploited interferograms with arcs; the sketch below shows the corresponding SCM where diagonal elements refer to the images and the filled off-diagonals represent the employed interferograms. Images are assumed to be temporally sorted. (a) partial exploitation of the data with short temporal baseline interferograms of up to band bw, and (b) the full exploitation of the interferograms with full SCM.

To explain the observed fading signal of our data set, in section IV-E we propose an alternative model to moisture variation. This analysis serves as an example to show that for a an effective calibration we either need to perform a comprehensive research on various possible physical sources of inconsistencies and design case-specific models to explain the interferometric phase of each source; or to design a generic model applicable to all possible sources of inconsistencies. In both cases, further studies on various test sites are inevitable. This model-based approach in reconstruction of consistency is subject to comprehensive research, hence, as of present, still inapt for systematic deformation monitoring.

A practical approach in reconstruction of consistency is to retrieve the consistent components of the phase within the time series, i.e. by explicitly imposing the condition of $\Delta\phi_{imk} = 0$ among all the $n(n-1)/2$ interferograms within the time series. This approach is initially designed to reduce the stochastic noise within the interferogram stack [5], [11]. However, as it will be revealed by the analysis of this paper, it significantly reduces the effect of systematic phase inconsistencies as well. Referred to as *phase linking*, the method is explained in section II-C. Phase linking does not consider a specific model for the fading signal, it rather gains robustness to such signals by exploring the temporal data redundancy of the interferograms. The success of phase linking in unbiased reconstruction of the consistency may lie in exploiting a sufficient number of interferograms in large data stack, and/or in the nature of the fading signals which are short-lived and tend to decorrelate over long time spans. The examination of these theses is beyond the scope of this paper. Within the scope of this paper, we substantiate that phase linking is an efficient and practical solution to reconstruct the consistency.

C. Phase linking techniques

After its pioneering authors, we define phase linking as the estimator which retrieves $n-1$ independent common-master interferograms from the partially redundant $n(n-1)/2$ multimaster interferograms [11]. Here we shortly introduce phase linking.

Without loss of generality, we concentrate on one DS region (see [5], [9] for algorithmic details of the DS region selection). The DS is comprised of an ensemble of spatially homogeneous region of p pixels in a time series of n SAR images, arranged in a matrix $\boldsymbol{Z} \in \mathbb{C}^{n\times p}$. Based on the central limit theorem, $\boldsymbol{Z}$ follows the zero-mean n-variate Complex Circular Gaussian (CCG) distribution [2]. Under the validity of this distribution, the sample covariance matrix, or its normalized version Sample Correlation Matrix (SCM), suffices for the full description of the DS. The SCM, denoted by $\boldsymbol{C}$, is a Hermitian matrix whose off diagonal elements pertain to all possible multilooked interferograms $\boldsymbol{I}_{ik}$ within the time series and their corresponding coherence $\boldsymbol{\Gamma}_{ik}$, i.e:

$$\angle \boldsymbol{C}_{ik} = \boldsymbol{I}_{ik} = \Delta\phi_{ik} \tag{3}$$

$$|\boldsymbol{C}_{ik}| = \boldsymbol{\Gamma}_{ik} \tag{4}$$

Various phase linking approaches are defined based on different modeling of the SCM [14], [15]. In an earlier work, we proposed a computationally efficient approach to phase linking called Eigen-decomposition-based Maximum-likelihood-estimator of Interferometric phase (EMI) [14]. This proposal decreases the computational cost by reformulating phase estimation into the following Eigen-decomposition problem [14]:

$$\hat{\boldsymbol{\phi}} = \angle(\text{argmin}_{v_i}\{\boldsymbol{v}_i^H\ (\boldsymbol{C}\circ\boldsymbol{\Gamma}^{-1})\ \boldsymbol{v}_i\}); \tag{5}$$
$$\text{subject to} \quad \boldsymbol{v}_i^H\boldsymbol{v}_i = 1$$
$$\text{and} \quad \boldsymbol{v}_i^H\boldsymbol{v}_k = 0;$$

where $\boldsymbol{v}_i$ is an arbitrary complex vector of size $n\times 1$ and $\circ$ is the Hadamard product.

$\hat{\boldsymbol{\phi}}$ is a vector of n wrapped phase values. It contains the consistent interferometric phase component within the exploited interferograms. This phase information is used for the retrieval of the deformation signal. EMI allows the convenient estimation of this phase series by taking the smallest Eigen vector of the matrix $\boldsymbol{C}\circ\boldsymbol{\Gamma}^{-1}$.

Note that, as common in InSAR, the estimation of absolute phase is ambiguous. An arbitrary image in the time series is selected as a reference scene, its phase is set to zero and the remaining phases are measured relative to this arbitrary datum.

III. Methodology in Accuracy Assessment

In this section we explain our experiments to reveal the existence and impact of the phase errors in multilooked interferograms. The design of these experiments is based on the following rationale:

- any systematic discrepancy between the single-look and multilooked observations is an indicator of fading signals (see section II-A);
- should inconsistent systematic effects exist within the multilooked interferograms, the deformation estimates vary depending on which interferograms are exploited.

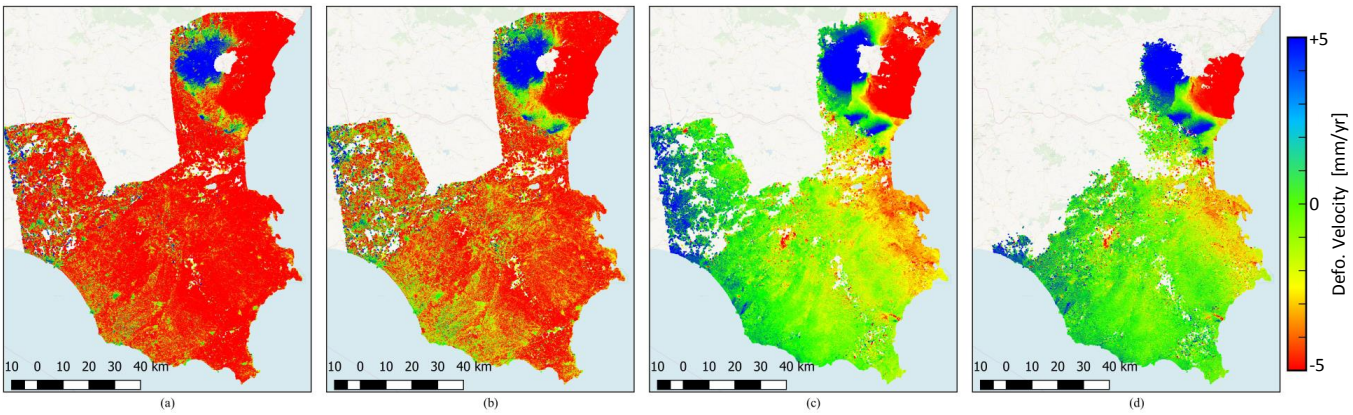

Fig. 2: displacement velocity maps of three different DS processing schemes (a) E-StBAS5 with $bw = 5$ (b) E-StBAS10 with $bw = 10$ (c) EMI using full SCM; as compared to (d) the benchmark PSI processing. The reference scene and reference point are identical in all maps.

As the benchmark of the experiments, we perform PSI to retrieve the deformation based on single-look observations. Exploiting various combination of multilooked interferograms, we further perform multiple processing rounds to investigate the impact on deformation estimates. In the first processing round, we exploit all possible interferograms within the time series as explained in section II-C. In the following processing rounds, we test the ingestion of different subsets of the interferograms; the corresponding estimator for this processing is introduced in section III-A.

As explained in section III-B, the resulting deformation estimates from the different processing schemes are evaluated against the benchmark PSI to study the estimation bias. In section III-C, we expand on our experiments to reveal the existence of the fading signals in multilooked interferograms and quantify their magnitude and impact on the deformation estimates.

A. Enhanced Short Temporal Baseline Subset Algorithm

To allow the ingestion of different subsets of interferograms and evaluate the impact on the deformation estimates, we designed a variation of the SBAS technique of [4]. The difference with respect to the conventional SBAS is two-fold:

- the baseline constrain is only imposed on the temporal separation between the acquisition pairs;
- phase linking is performed on the chosen interferogram subset. Deformation estimation follows based on the wrapped phase estimates.

Refraining from unwrapping the interferograms and performing phase linking on the subset instead, the designed approach is less prone to the propagation of phase unwrapping errors. To reflect these difference with the conventional method, we refer to this approach as Enhanced Short temporal BAseline Subset algorithm (E-StBAS).

The chosen interferogram subset is comprised of bw number of shortest temporal baseline interferograms per acquisition in the time series. Such that the total number of the exploited interferograms reads as:

$$m = \frac{bw}{2}(2n - bw - 1) \tag{6}$$

Compared to the conventional phase linking, here a band matrix will replace the full SCM (see Fig. 1). The bandwidth of the matrix is defined by the parameter bw. The consistent phase based on these interferograms is reconstructed via the following iterative optimization:

$$\hat{\boldsymbol{\phi}}_i^p = \angle\left(\frac{1}{bw}\sum_{k=1}^{bw}\boldsymbol{\Gamma}_{i,i+k}\exp(j\Delta\phi_{i,i+k} - j\hat{\boldsymbol{\phi}}_{i+k}^{p-1})\right) \tag{7}$$

The iterations can be initialized by the largest Eigen vector of the band matrix $\boldsymbol{C}^{bw}$, i.e.:

$$\begin{aligned} & \hat{\boldsymbol{\phi}}^0 = \angle(\text{argmax}_{\boldsymbol{v}_i}\{\boldsymbol{v}_i^H\boldsymbol{C}^{bw}\boldsymbol{v}_i\}); \\ \text{subject to} \quad & \boldsymbol{v}_i^H\boldsymbol{v}_i = 1, \\ \text{and} \quad & \boldsymbol{v}_i^H\boldsymbol{v}_k = 0. \end{aligned} \tag{8}$$

In practice (8) provides a sufficient approximation such that the iteration by (7) is unnecessary. As in section II-A, $\hat{\boldsymbol{\phi}}$ contains the consistent interferometric phase component within the exploited subset. This phase information is used for the retrieval of the deformation signal.

B. Evaluation of Deformation Bias

Retrieving the consistent phase series for DS using either EMI or E-StBAS, the standard PSI processing [1], [16] is employed on the high SNR DS to initially mitigate the atmosphere and eventually estimate the deformation [5]. Two products may be retrieved from the deformation signal, namely the relative displacement time series of size $n-1$ per DS, and more concisely the modeled displacement velocity as a single parameter per DS.

The intention is to evaluate the accuracy of both DS-derived products. We opt for the PS deformation measurements as the benchmark for validation.

The performance evaluation is conducted as following: a spatial grid of size 1 km^2 is chosen for down-sampling both displacement time series and displacement velocity maps. Signal stationarity is assumed within this spatial window. For all PS and DS within the defined reference grid cells, a weighted average of the deformation signal substitutes the sparse estimates. The weighting is based on the a posteriori

coherence of PS [16] and DS [5]. For the latter scatterers, the clutter is disregarded using a constant false alarm rate detector. Following this approach the down-sampled DS and PS deformations are directly comparable. From this point on, the calculation of the estimation bias in deformation products is straight-forward:

$$\epsilon_{d(x,y)} = \langle d_{\mathrm{DS}(x,y)} \rangle - \langle d_{\mathrm{PS}(x,y)} \rangle \tag{9}$$

here $\langle . \rangle$ shows the mentioned weighted averaging operator, x, y are the spatial coordinates of the down-sampled grid and ϵ_d is the evaluated bias. Subscript d can represent either the displacement values in the time series or the displacement velocity.

This evaluation will result in a time series of displacement bias as well as the overall displacement velocity bias for the entire time series. Both biases are calculated over the down-sampled spatial grid.

C. Evaluation of Interferometric Phase bias

We intend to track the bias in displacement velocity to the exploited multilooked interferograms. We firstly introduce a measure to quantify the interferometric phase bias which pertains to the fading signals. Using error propagation we introduce a second measure to calculate the expected displacement velocity bias from the phase biases.

In the introduction of our first measure, we assume to know the interferometric phase $\Delta\tilde{\phi}$ which is free of the systematic and stochastic inconsistencies (see section II-A). Knowing this phase, the error of the multilooked interferograms can be evaluated for each DS at each interferogram, i.e.:

$$\epsilon_{\Delta\phi_{ik}(x,y)} = \Delta\phi_{ik(x,y)} - \Delta\tilde{\phi}_{ik(x,y)}. \tag{10}$$

Here $\Delta\phi$ shows the multilooked phases over DS regions, subscripts i, k refer to the master and slave acquisition index and x, y are the spatial coordinates of the DS. The phase $\Delta\tilde{\phi}$ can be substituted e.g. by high SNR single-look observations (see section IV-D for the practical approach to evaluation of phase error).

In principle one can estimate the phase bias from the phase errors by allowing an averaging operator on a chosen ensemble; the averaging is necessary to reduce the stochastic noise. In our bias estimation, we choose a temporal averaging within the time series. The averaging is performed on the calculated phase error of each DS within the interferograms with identical time lag l separation from their respective master scene. A normalization with respect to the temporal baseline of the interferograms is further considered. Following the temporal averaging and baseline normalization, the intended measure reads as:

$$\delta^l{}_{(x,y)} = \frac{1}{n-l} \sum_{i=1}^{n-l} \frac{\epsilon_{\Delta\phi_{i,i+l}(x,y)}}{\Delta t_{i,i+l}}. \tag{11}$$

δ^l is the average phase bias of each DS region per time lag l. The temporal normalization allows the direct comparison of the calculated phase biases without the concern for their variable temporal baseline. It as well eases the error propagation from the interferogram level to the displacement velocity, as explained in the following.

TABLE I: Summary of the compared approaches for the estimation of displacement velocity. PSI is used for the evaluation of bias and dispersion.

Phase Estimation	SCM Bandwidth bw	Estimation Bias [mm/yr]	Estimation Dispersion [mm/yr]
E-StBAS5	5	-6.50	2.58
E-StBAS10	10	-3.05	1.55
EMI	full SCM	-0.24	0.70

We further quantify the expected bias in the displacement velocity given the biases of interferograms by introducing a second measure. To commence, let us simplify the phase reconstruction of (7) by assuming uniform weighting, i.e. $\forall i, k \in \{1, ..., n\} : \mathbf{\Gamma}_{ik} = 1$. Further, we assume the phase errors are small enough that the small-angle approximation holds i.e. $\angle \exp(j\epsilon_{\Delta\phi}) \approx \epsilon_{\Delta\phi}$. Furthermore, the mentioned temporal normalization of (11) is necessary to propagate the phase bias to displacement velocity bias. Following the mean propagation law for linear models [17], the displacement velocity bias reads as:

$$\epsilon_{d_{\mathrm{vel}}(x,y)} = \frac{1}{bw} \frac{\lambda}{4\pi} \sum_{k=1}^{bw} \delta^k{}_{(x,y)}, \tag{12}$$

where λ is the radar wavelength. To recapitulate, the introduced error propagation assumes that:

- the present phase error of the multilooked observations is small;
- all interferograms are equally weighted in phase estimation.

The first simplification holds for short temporal baselines where the decorrelation noise is negligible enough not to violate the small-angle approximation. The second simplification is more likely to have an effect on the estimation of the phase and displacement velocity bias. Nevertheless, $\epsilon_{d_{\mathrm{vel}}}$ provides a mean to verify the evaluated biases of section III-B with the predicted displacement velocity bias from the phase errors in multilooked interferograms. In case of positive verification, we may conclude that the cause of deformation biases stems from the multilooked interferograms and rule out other plausible sources in raising the deformation biases.

IV. Analysis of Biases

For the study of the biases, a test site is chosen in the island of Sicily-Italy. The test site is regularly monitored by Sentinel-1 A and B, providing abundant data. The land cover is heterogeneous to observe the behavior of different DS types. The area is investigated by different studies, such as [18], [19], which potentially allows independent performance comparison.

The data set is comprised of 184 acquisitions from October 2014 to September 2018 of descending track. It covers approximately 15000 km^2.

Following the introduced methods in section III, the biases in displacement time series and velocity as well as the multilooked interferograms are studied in this section.

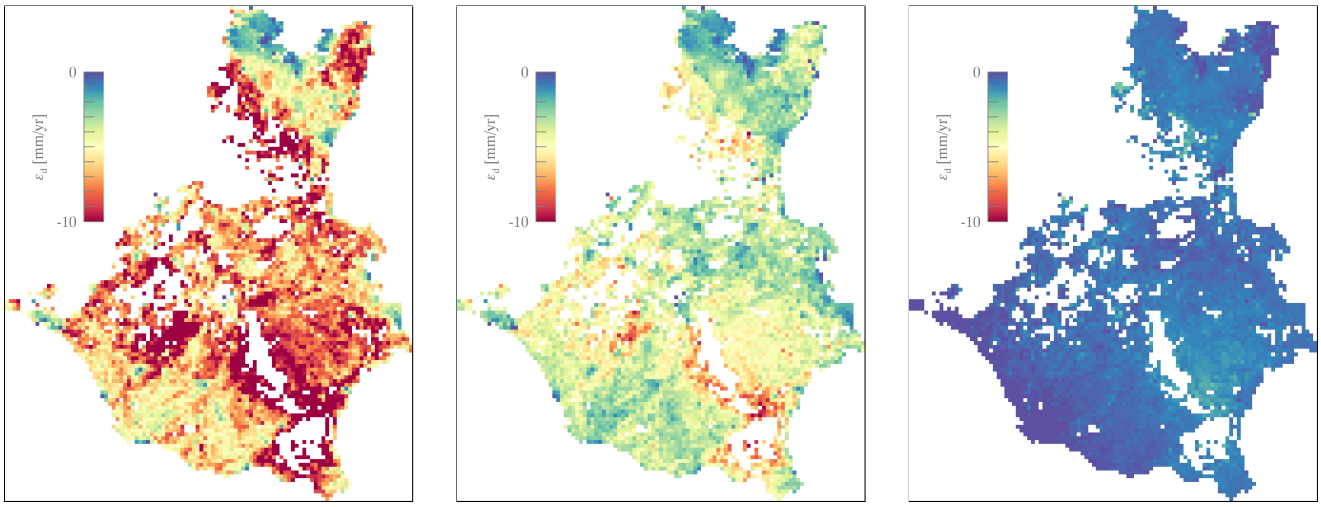

(a) (b) (c)

Fig. 3: Displacement velocity bias $\epsilon_{d_{\text{vel}}}$ estimated according to (9) for (a) E-StBAS5, (b) E-StBAS10, (c) EMI using full SCM.

A. The comparison scenarios

The intention is to define a scientifically credible experiment which can isolate the impact of multilooked phases on deformation estimation.

We perform three different DS analysis for deformation retrieval. All steps of the processing and the corresponding latent parameters are kept identical, the only difference is in consistency reconstruction (see section II-B). With reference to section II-C and III-A, different number of interferograms and different phase estimation methods are used to retrieve the consistent interferograms, namely:

- E-StBAS with bandwidth of five;
- E-StBAS with bandwidth of ten;
- EMI performing phase linking on full SCM.

The defined experiment is summarized in table I.

Identical to the three cases, Interferometric Wide Area Processing (IWAP) chain [20] is used for deformation estimation, the estimation of consistent interferograms is integrated in this chain. As the first step toward DS processing, the statistically homogeneous ensembles surrounding each pixel are detected. The amplitude-based Anderson-Darling statistical similarity test [9] with false alarm rate of 5% is chosen as the detection method. The search window for the test comprises of 25 and 7 looks in range and azimuth direction, respectively. The effective number of look is however approximately half in each direction. The homogeneous ensembles are exploited for adaptive multilooking of the direct interferograms as well as estimation of the SCM at DS region. A constant false alarm rate detector is further used to detect the signal bearing DS and exclude the low quality regions from the deformation analysis [21]. The latter regions pertain to fast decorrelating scatterers such as water bodies and dense vegetation.

Beside the above-mentioned three DS comparison cases, we perform a conventional PSI [16] and treat the result as the benchmark for our analysis to follow.

Note that in the overall four processing rounds, the reference scene and reference point are identical. Moreover, the latent parameters are kept identical or chosen in data-driven fashion, to ensure the credibility of the comparisons.

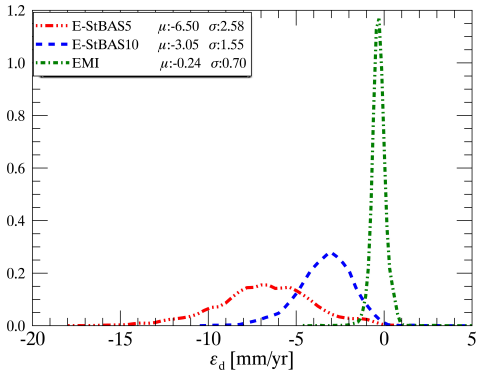

Fig. 4: Empirical PDF of displacement velocity bias evaluated by (9), reported for the three DS processing schemes. The first μ and second σ order moments of these Empirical PDFs indicate the overall bias and dispersion of the velocity estimates, respectively. The increase in the number of exploited interferograms improves the overall accuracy of deformation estimation.

Fig. 2 shows the retrieved displacement velocity map of these four described schemes. In the following sections, the results are quantitatively analyzed.

B. Bias in displacement velocity

We are interested in the quantitative error of the displacement velocity maps reported in Fig. 2. Following the described method in section III-B, the PS scheme is taken as the benchmark. According to (9), the discrepancy between the velocity estimated by each three DS schemes are evaluated against this benchmark over a down-sampled grid. Fig. 3 depicts the evaluated $\epsilon_{d_{\text{vel}}}$ of each scheme over the test site. Fig. 4 depicts the Empirical probability density function (PDF) of the accumulated discrepancies over the entire test site. The first and second order moment of these PDFs provide a measure for the overall bias and dispersion of each method in the estimation of the displacement velocity. These performance indicators are summarized in table I.

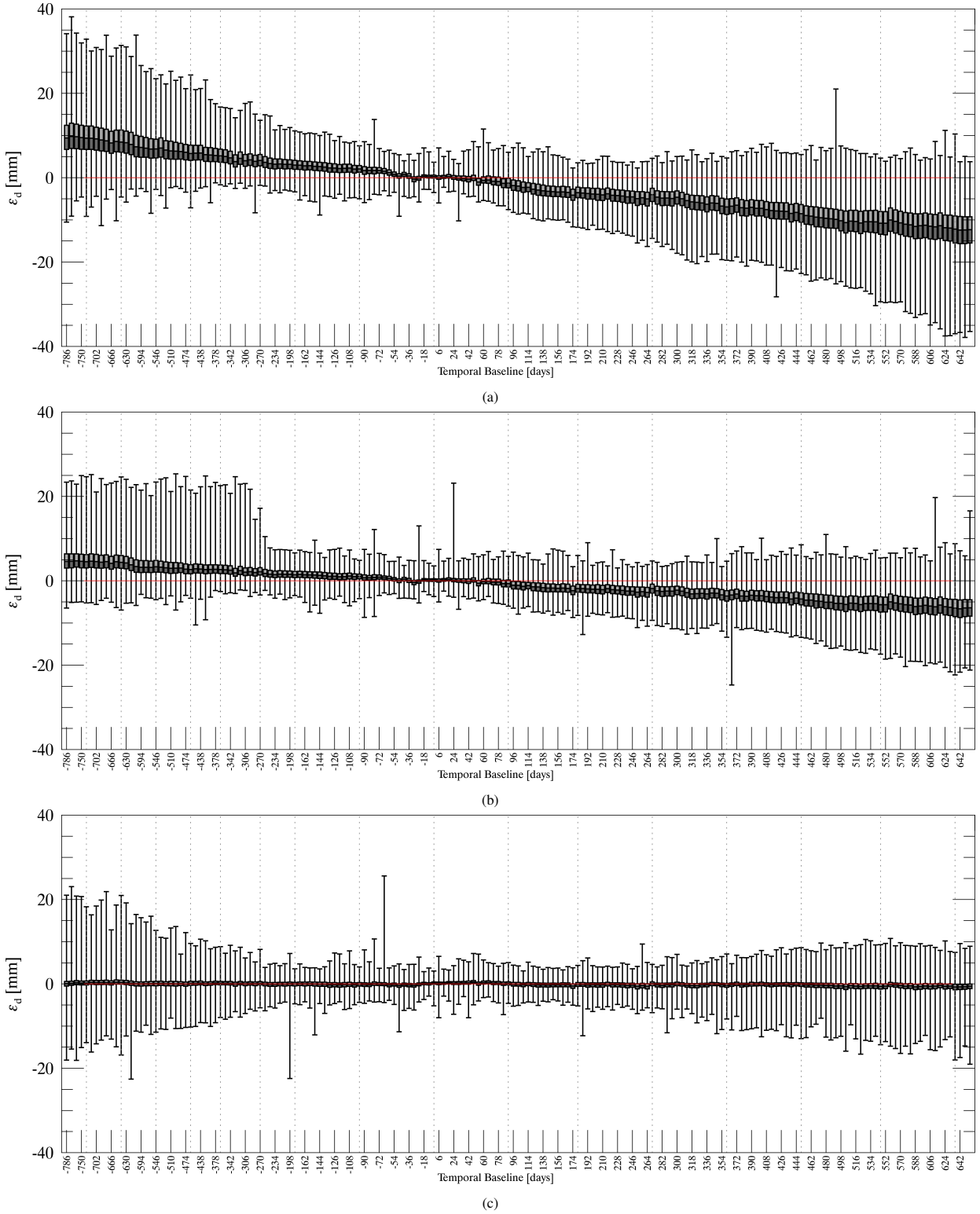

Fig. 5: The box-whisker plots of displacement error for each acquisition in the time series, with respect to its temporal baseline, presented for different DS processing schemes of (a) E-StBAS5, (b) E-StBAS10, and (c) EMI scheme on full SCM. The bias and dispersion of the displacement estimates is inferred from the boxplot. Both performance measures improve by including more interferograms in phase estimation.

As revealed by the comparisons, both the bias and dispersion decrease when more interferograms are exploited for phase and consequently deformation estimation. The overall performance of E-StBAS techniques is observed to be worse than the achievable precision of 1-2 mm/yr for Sentinel-1 data stacks [22], [23], while the exploitation of full covariance matrix helps EMI in retaining this potential performance.

C. Bias in displacement time series

We further extend the bias analysis by evaluating the discrepancy in the displacement time series. The latter time series is the outcome of spatiotemporal phase unwrapping and the removal of the estimated topographic and atmospheric signal components.

Similar to the previous section and following the method of section III-B, the displacement bias between each DS scheme and the benchmark PSI result is evaluated for each available time epoch. The displacement bias is therefore evaluated per acquisition and over the down-sampled grid via (9).

For a compact visualization of the temporal behavior, box-whisker diagrams are chosen here. Each diagram represents the spatially accumulated bias measures for each acquisition in the stack. The diagram provides a robust presentation of the distribution of univariate data. The box represents the 50% concentration of the data. The whiskers show the extent of distribution within 80% confidence interval. The box-whisker diagram concisely depicts the following robust statistical measures:

- median: marked by the central line of the box. It is a robust measure of the average displacement bias;
- interquartile range: visible from the length of the rectangular box. It is a robust measure for the dispersion of the displacement estimates;
- skewness: inferred from the asymmetry between the upper and lower parts of box-whisker around the median. Skewness is the third moment of data as a measure for the normality of the distribution of displacement error. A skewed distribution indicates a systematic discrepancy between the PS and DS.

Fig. 5 depicts the box-whiskers for the three compared DS schemes. The average displacement bias of each acquisition is provided in Fig. 6. The following conclusions are drawn from the three mentioned figures:

- both the bias and dispersion of the displacement estimates increase with the temporal baseline. The error propagation is more severe where less interferograms are exploited;
- a prevailing linear trend is observed for E-StBAS5 and 10, implying the persistent presence of physical source of bias in the DS over the entire time series;
- the overall skewness of the box-whiskers reduces in EMI, as compared to E-StBAS5 and E-StBAS10, indicating the reduced systematic errors in EMI;
- a small periodic trend is observed which may be attributed to the moisture variations [7], [13];
- exploiting all multimaster interferograms and applying EMI for the reconstruction of consistency significantly reduces the bias in displacement estimation.

D. Tracking the bias to multilooked interferograms

Up to this point, we observed an increased bias in the displacement velocity as well as a prevailing presence of a linear physical signal in the displacement time series. The observed signals are absent in the result of single-look PS measurements

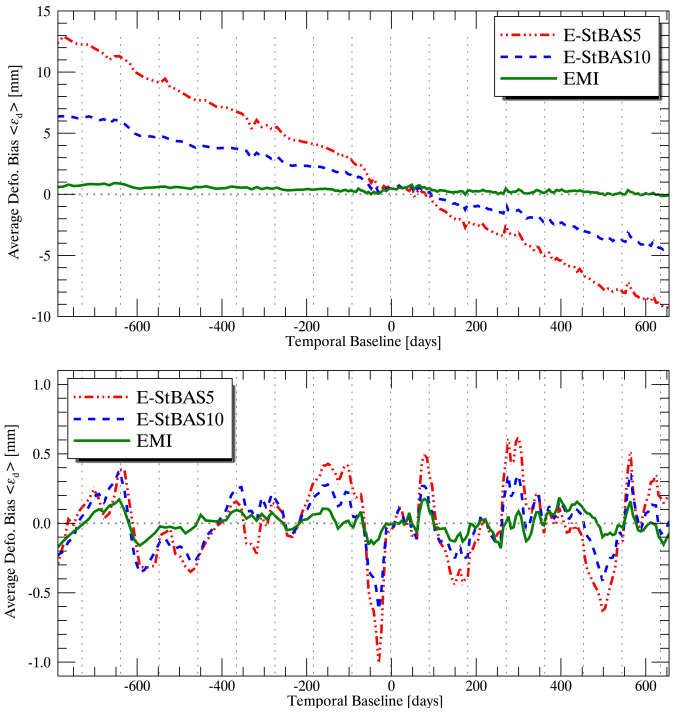

Fig. 6: Temporal trends of the average bias in displacement estimation for the three compared DS schemes. top: the overall trend, bottom: the periodic behavior resulted from the removal of the linear trends. The linear variation of the displacement bias prevails the periodic changes. This implies the negligible effect of seasonal variations of the phase which are attributed to the moisture variation.

and fade when exploiting all the interferograms within the time series, therefore they can not be justified as surface topography change. In this section we seek for the cause of this linear trend in the direct multilooked interferograms and attempt to predict the error budget in displacement velocity from the phase bias of the mentioned interferograms.

Following the method of section III-C, the focus here is on the quantification of interferometric phase bias at varied time lags. Note that according to (10) and (11), $\Delta\tilde{\phi}$ is required for the evaluation of the phase error. From the analysis of the previous subsections, we observed a negligible sub-millimetric discrepancy between the single-look PS measurements and the estimated phases of EMI approach. Therefore, we may approximate the single-look PS phases by the estimated phases based on the full SCM, i.e. the EMI result, and use the latter as the benchmark $\Delta\tilde{\phi}$ for the evaluation of phase bias. Having this benchmark, δ^l is evaluated for $\forall l \in \{1, ..., 10\}$. Fig. 7.a and b depict an example of the estimated phase biases for $l = 1$ and $l = 10$. These time lags correspond to the average temporal baseline of 8 and 78 days, respectively (we resorted to the calculation of the average temporal baseline for each time lag, due to the irregular temporal acquisition of the images). The empirical PDF of the spatially accumulated δ^l measures for variable time lags are provided in Fig. 7.c.top, the bottom figure provides the evolution of the average phase bias over time. From these observation, we conclude that the short temporal interferograms, with smaller time lag l, are more biased as compared to the longer baselines. This observed

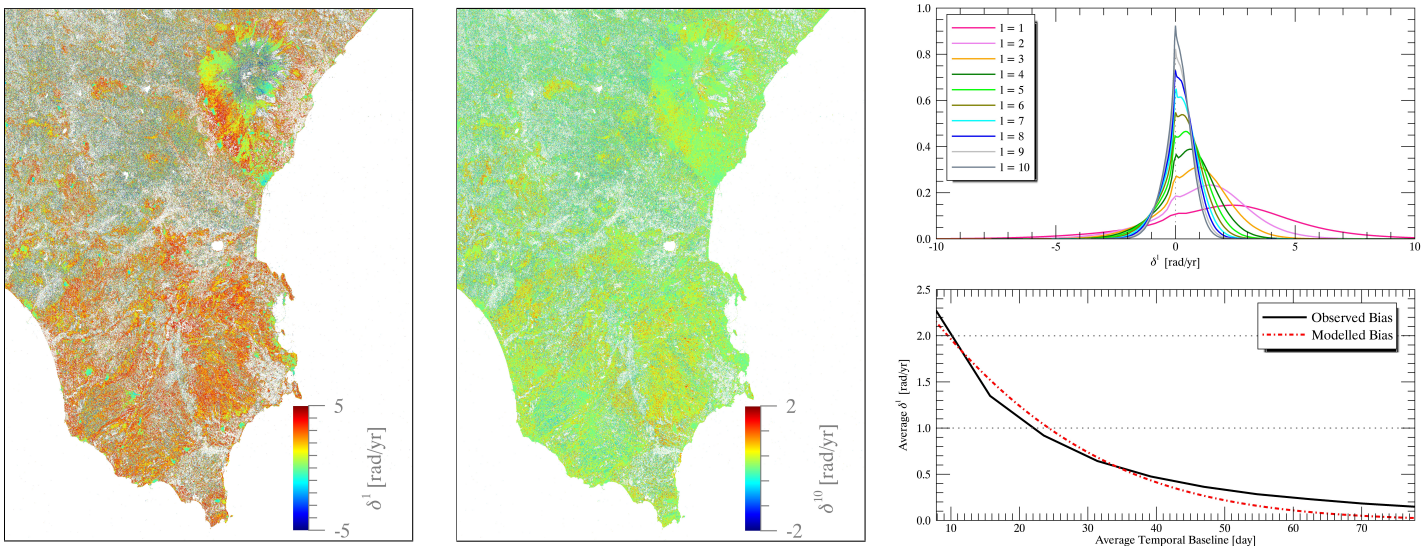

(a) $l = 1$ (b) $l = 10$ (c)

Fig. 7: Evaluation of systematic phase bias for different interferograms via δ^l of (11) (a) overall bias for temporal lag of $l = 1$ equivalent to average temporal baseline of 8 days, (b) overall bias for temporal lag of $l = 10$ equivalent to average temporal baseline of 78 days, (c) top: empirical PDF of spatially accumulated δ^l measures per time lag and bottom: the average phase bias as a function of the temporal baseline. Contrary to the general perception, the shorter temporal baseline, and therefore more coherent, interferograms are observed to be more biased. The bias decreases with temporal baseline.

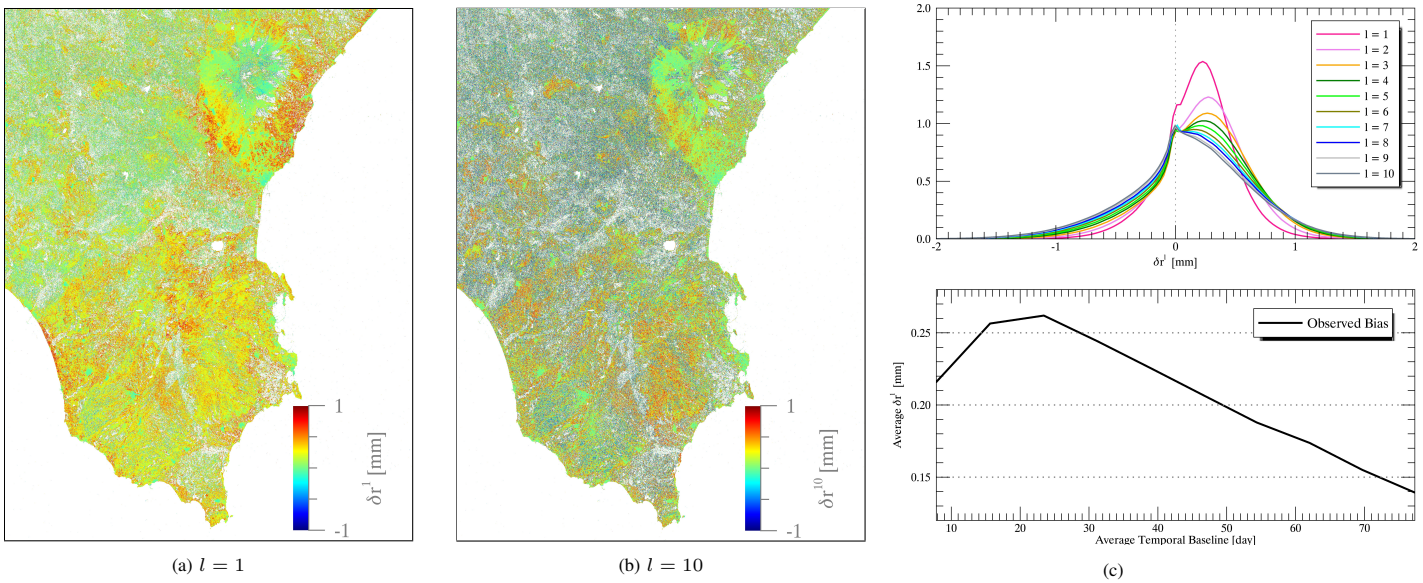

(a) $l = 1$ (b) $l = 10$ (c)

Fig. 8: Evaluated observed bias in slant range corresponding to the systematic phase bias of Fig. 7.a and b. for temporal lag of (a) $l = 1$ equivalent to average temporal baseline of 8 days, (b) $l = 10$ equivalent to average temporal baseline of 78 days. (c) top: empirical PDF of spatially accumulated δr^l measures per time lag and bottom: the average phase bias as a function of the temporal baseline. The biases are sub-millimetric and small compared to the atmospheric perturbations. The propagation of these small biases compromises the performance of E-StBAS processing schemes.

trend will assist us in the proposal of a simple physical model for the source of phase biases in section IV-E.

According to section III-C, the phase bias of multilooked interferograms is propagated to the displacement velocity estimates via (12). From the integration of the δ^l measure and their proper normalization and conversion, $\epsilon_{d_{\text{vel}}}$ is further evaluated for the two processing schemes of E-StBAS5 and E-StBAS10. Fig. 9 shows the predicted displacement velocity bias based on the observed phase biases. The empirical PDF of the accumulated $\epsilon_{d_{\text{vel}}}$ measures in Fig. 9.c provides the average bias of these processing schemes over the test site. The predicted bias reads as 5.43 and 3.38 mm/yr for the E-StBAS5 and 10 respectively. Comparing these biases to the empirical values from the bias estimates of table I confirms that the measured biases in the deformation estimates are caused by the interferometric phase biases. Note that the discrepancy between the predicted and the empirical displacement velocity bias is due to two approximations: firstly the underlying simplification of the error propagation scheme (explained in section III-C) and secondly the approximation of $\Delta\tilde{\phi}$ by the reconstructed phases of EMI. The sign change between the predicted and empirical values only stems from the difference

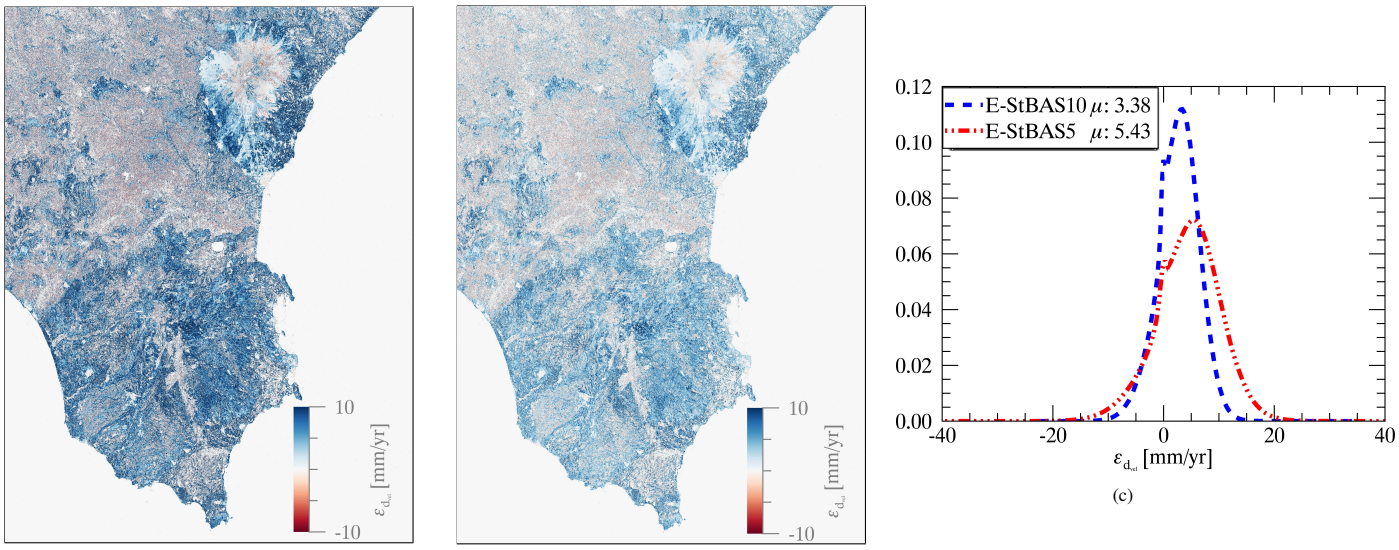

(a) $bw = 5$ (b) $bw = 10$

Fig. 9: The predicted error in displacement velocity via $\epsilon_{d_{\text{vel}}}$ of (12): (a) E-StBAS5 scheme, (b) E-StBAS10 scheme, and (c) the empirical PDF of spatially accumulated error measures. The deformation velocity bias is predicted as 3.38 and 5.43 mm/yr for E-StBAS10 and E-StBAS5, respectively. These values corroborate the empirical biases of -3.05 and -6.50 mm/yr with our real data analysis, as seen in Fig. 4 and table I. The sign change between the predicted and empirical values only stems from the difference in the convention for setting the direction of positive displacement.

in the convention for setting the direction of positive displacement.

E. Modeling of phase bias

Having corroborated the presence of a systematic bias in multilooked interferograms, in this section we seek a model that can explain the fading signals and the corresponding phase biases. Upon comprehensive study of such models, they may be used in model-based reconstruction of phase consistency as explained in section II-B.

Our first attempt in modeling was to explain the bias with the moisture model of [12]. However the sign of the deformation bias is not justifiable with the moisture model. If there is a bias from the moisture cycle, this should appear as a motion *towards* the satellite. This happens because the typical behavior is for soils to get wet fast and dry slowly. Our non-linear model for the moisture phase, confirmed by observations in real data, predicts that the cumulative phase change corresponding to a certain moisture change is larger if the change is observed through many small steps that if it happens suddenly or through larger steps. Therefore slow drying (moving apparently towards the satellite) should prevail over fast wetting. If a moisture bias is present, it is overshadowed by some other biasing signal.

An alternative hypothesis is that we are observing biomass growth, with an apparent motion away from the satellite which introduces extra range delay. Based on this hypothesis, a model is proposed which is comprised of two parts; that is, a linear systematic phase variation ρ_ϕ and a temporal decorrelation to explain the vanishing bias with longer baselines.

To introduce this model, consider the temporal decorrelation model of [24]:

$$\Gamma_{i,k} = (\gamma_0 - \gamma_\infty)\,\exp(-|\delta t_{i,k}|/\tau)\; + \gamma_\infty; \qquad (13)$$

with γ_0 and γ_∞, respectively, as the short-term decaying and long-term persistent coherence of an arbitrary interferogram; δt as its temporal baseline and τ as the signal correlation length. This model is generalized to include the systematic phase variation:

$$I^{\text{sys}}_{i,k} = (\gamma_0 - \gamma_\infty)\exp(j\ \rho_\phi\ \delta t_{i,k})\exp(-|\delta t_{i,k}|/\tau) + \gamma_\infty \quad (14)$$

where ρ_ϕ corresponds to rate of phase variation in radians over time. The phase of this complex model explains the observed phase bias in an arbitrary interferogram pair.

In Fig. 9.c.bottom we modeled the observed average phase bias $\langle \delta^l \rangle$, considering the average temporal baseline for each time lag. Using the simple model of (14), a weak systematic signal with short and long term coherence of 0.28 and 0.21, correlation length of $\tau = 19.5$ days and variation of $\rho_\phi = 0.03$ rad/day is captured in the data set.

The modeled apparent motion of 0.03 rad/day corresponds to almost 50 mm/yr of extra range delay. Converted to water, which must be the main responsible for the delay, it totals 5.3 mm/yr (= 5.3 $\text{l}/(\text{m}^2\text{yr})$ or $\text{kg}/(\text{m}^2\text{yr})$) of water, assuming a relative dielectric constant of 80. This seems to be a reasonable figure for a first plausibility check of the proposed biomass growth model. A more realistic model needs to relate water to total or dry biomass and to consider that the interferometric phases are implicitly weighted by backscatter intensities. Nonetheless, the simple model of (14) provides an approximation and justifies the correct sign of the phase bias.

The generalization, validation and use of this proposed model for the calibration of phase biases is subject to further research.

V. Discussion and Recommendations

In this paper we primarily focused on the observation of a peculiar systematic signal in InSAR. Concluding that:

- multilooked interferograms reveal a short-lived, systematic phase component which cannot be attributed to atmospheric or surface topography variations. This systematic phase component is absent in single-look phase observations;
- phase biases are larger for shorter temporal baseline, albeit more coherent, interferograms;
- the magnitude of the phase bias in each multilooked interferogram may be deemed small, especially compared to the atmospheric perturbations. However, with the attenuation of atmospheric phase and the propagation of the interferograms phase bias within the time series, the corresponding error for the displacement velocity estimation is alarming;
- the propagation of even small phase biases in long time series compromises the accuracy of displacement velocity maps from an achievable sub-millimetric to centimetric per year level.

Studying the effect of the observed signal for interferogram time series, we established that:

- the redundancy of multimaster interferograms is decreased as the result of the present systematic signals;
- exploiting the temporal data redundancy in large time series yields a degree of robustness of the phase retrieval algorithms to such phase errors;
- the major role in the gained robustness is played by the inclusion of the long temporal baseline interferograms in phase retrieval.

Moreover, we shortly discussed the possibility of modeling the phase biases:

- for the region under study, the systematic phases comprise of a prominent linear and a much lower magnitude periodic signal;
- the periodic phase may be attributed to the change in moisture variation of the subsurface medium;
- a complex decorrelation model is proposed as an approximation of the linear systematic trend;
- the proposed decorrelation model helps in the interpretation of the physical phenomenon behind the systematic phase component. However, as of present, we lack adequate experimentation and validation of this simplified model for the calibration of phase biases;
- the observed fading signals are specific to the chosen test site. Understanding the physical sources of these signals in multilooked interferograms is subject to comprehensive research;
- due to the lack of comprehensive research thus far, the use of model-free phase linking in the mitigation of phase errors is one of the most viable approaches in safeguarding against the fading signals.

As hypothesized, the presence of fading signal compromises the accuracy of InSAR in deformation analysis. This problem is highly exacerbated for Big Data processing. Common practice in such processing is to mostly exploit short temporal baseline interferograms [19], [25], [26]. The logic behind such data exploitation is to reduce the number of interferograms by using the most coherent, and thereby highest SNR, observations in the time series. However, the analysis of this paper proves that these interferograms are the most affected by the inconsistent fading signals and therefore the least reliable for deformation retrieval. This observation challenges the quality of the short temporal interferograms and warns against solely using these observations.

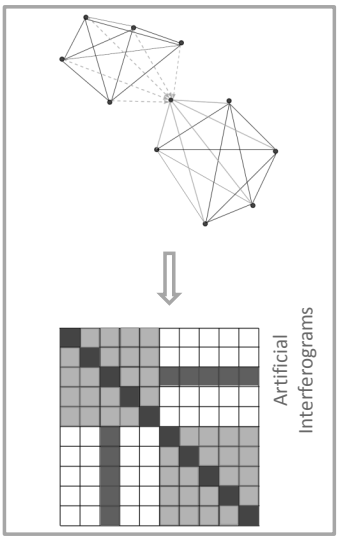

Fig. 10: Efficient exploitation of Big Data stacks using the Sequential Estimator [27]. With reference to Fig. 1, the sequential estimator divides the data stack into isolated batches. Between batches, the lost information is retrieved by the formation of compressed images (shown by the dot in between the two fully connected networks) and the artificial interferograms depicted with the respective arcs and dark shaded in the SCM. The dashed arcs represent the contribution of isolated batches in formation of the compressed images. Following this rationale, the full SCM of Fig. 1.b is recursively approximated to avoid redundant calculations while retaining the accuracy in phase estimation.

Should the small baseline processing scheme be desired for deformation retrieval, we recommend to safeguard against the impact of systematic phase biases by:

- exploiting the long temporal baseline interferograms along with the short ones to decrease the overall phase error;
- predicting deformation error budgets following the analysis of section III-C and according to (12); choosing the optimum number of interferograms (i.e. the bw parameter) for achieving a desired accuracy. The phase series pertaining to single-look PS could be the benchmark for such error prediction.

According to our experiments, however, the choice of optimum number of interferograms for reliable deformation estimates is land cover dependent. For a single test site, various number of optimum interferograms may be discovered for different types of DS. Furthermore, the additional analysis on the optimum number of interferograms increases the computational burden of processing.

For reliable deformation monitoring, we advocate the use of phase linking on full SCM. This approach is fully data-adaptive. Contrary to the general belief, phase linking can be computationally efficient. According to our extensive wide

area processing experience, partially reported in [28], [29], EMI provides a viable efficient solution for phase linking and does not pose a challenge for Big Data processing. To avoid the redundant computations of phase linking in stream processing of large time series, we further recommend our proposal of sequential estimator [27] (see Fig. 10). The sequential estimator is based on data compression, it significantly reduces the number of exploited interferograms while retaining the capability to robustly reconstruct the consistency. The accuracy of this sequential algorithm is studied and proven to retain the millimeter per year level target [28].

Our final recommendation for insuring the accuracy in deformation monitoring is to introduce a new intermediate product level for InSAR, namely the reconstructed consistent wrapped phase series using EMI and the sequential estimator. The envisioned product would:

- contain the consistent physical signal components such as, but not limited to, atmospheric variations and surface displacements;
- significantly reduce the interferometric phase bias and stochastic noise, thereby enhance the reliability of InSAR for deformation retrieval;
- reduce the amount of interferometric data from the $n(n-1)/2$ pairwise interferograms within the data stack to a time series of $n-1$ higher quality and, optionally, downsampled interferograms;
- provide a unified product for accurate deformation monitoring to the user community.

This paper was dedicated to the analysis of C-band SAR. The magnitude of fading signals, and hence the corresponding errors, are expected to increase with the wavelength. Therefore larger effects are expected and observed for L-band SAR [7], rendering the introduced phase product even more essential to L-band.

REFERENCES

[1] A. Ferretti, C. Prati, and F. Rocca, "Permanent scatterers in SAR interferometry," *IEEE Transactions on Geoscience and Remote Sensing*, vol. 39, no. 1, pp. 8–20, Jan. 2001.

[2] R. Bamler and P. Hartl, "Synthetic aperture radar interferometry," *Inverse Problems*, vol. 14, no. 4, pp. R1–R54, Aug. 1998.

[3] N. Adam, A. Parizzi, M. Eineder, and M. Crosetto, "Practical persistent scatterer processing validation in the course of the Terrafirma project," *Journal of Applied Geophysics*, vol. 69, no. 1, pp. 59–65, 2009.

[4] P. Berardino, G. Fornaro, R. Lanari, and E. Sansosti, "A new algorithm for surface deformation monitoring based on small baseline differential sar interferograms," *IEEE Transactions on geoscience and remote sensing*, vol. 40, no. 11, pp. 2375–2383, 2002.

[5] A. Ferretti, A. Fumagalli, F. Novali, C. Prati, F. Rocca, and A. Rucci, "A New Algorithm for Processing Interferometric Data-Stacks: SqueeSAR," *IEEE Transactions on Geoscience and Remote Sensing*, vol. 49, no. 9, pp. 3460–3470, Sep. 2011.

[6] W. Gong, A. Thiele, S. Hinz, F. Meyer, A. Hooper, and P. Agram, "Comparison of small baseline interferometric sar processors for estimating ground deformation," *Remote Sensing*, vol. 8, no. 4, p. 330, 2016.

[7] F. De Zan, M. Zonno, and P. Lopez-Dekker, "Phase Inconsistencies and Multiple Scattering in SAR Interferometry," *IEEE Transactions on Geoscience and Remote Sensing*, vol. 53, no. 12, pp. 6608–6616, Dec. 2015.

[8] R. Lanari, O. Mora, M. Manunta, J. Mallorqui, P. Berardino, and E. Sansosti, "A small-baseline approach for investigating deformations on full-resolution differential SAR interferograms," *IEEE Transactions on Geoscience and Remote Sensing*, vol. 42, no. 7, pp. 1377–1386, Jul. 2004.

[9] A. Parizzi and R. Brcic, "Adaptive InSAR Stack Multilooking Exploiting Amplitude Statistics: A Comparison Between Different Techniques and Practical Results," *IEEE Geoscience and Remote Sensing Letters*, vol. 8, no. 3, pp. 441–445, May 2011.

[10] S. Zwieback, X. Liu, S. Antonova, B. Heim, A. Bartsch, J. Boike, and I. Hajnsek, "A Statistical Test of Phase Closure to Detect Influences on DInSAR Deformation Estimates Besides Displacements and Decorrelation Noise: Two Case Studies in High-Latitude Regions," *IEEE Transactions on Geoscience and Remote Sensing*, vol. 54, no. 9, pp. 5588–5601, Sep. 2016.

[11] A. Monti Guarnieri and S. Tebaldini, "On the Exploitation of Target Statistics for SAR Interferometry Applications," *IEEE Transactions on Geoscience and Remote Sensing*, vol. 46, no. 11, pp. 3436–3443, Nov. 2008.

[12] F. De Zan, A. Parizzi, P. Prats-Iraola, and P. López-Dekker, "A SAR interferometric model for soil moisture," *IEEE Transactions on Geoscience and Remote Sensing*, vol. 52, no. 1, pp. 418–425, 2013.

[13] F. De Zan and G. Gomba, "Vegetation and soil moisture inversion from SAR closure phases: First experiments and results," *Remote sensing of environment*, vol. 217, pp. 562–572, 2018.

[14] H. Ansari, F. De Zan, and R. Bamler, "Efficient phase estimation for interferogram stacks," *IEEE Transactions on Geoscience and Remote Sensing*, vol. 56, no. 7, pp. 4109–4125, May 2018.

[15] H. Ansari, F. De Zan, G. Gomba, and R. Bamler, "EMI: efficient temporal phase estimation and its impact on high-precision InSAR time series analysis," in *Proc. IEEE Geoscience and Remote Sensing Symposium IGARSS*, Yokohama, Japan., 2019.

[16] B. M. Kampes, *Radar Interferometry Persistent Scatterer Technique*. Springer Netherlands, 2006.

[17] P. Teunissen, D. Simons, and C. Tiberius, "Probability and observation theory." 2004.

[18] I. Zinno, M. Bonano, S. Buonanno, F. Casu, C. De Luca, R. Lanari, M. Manzo, M. Manunta, and G. Zeni, "Surface deformation mapping of italy through the P-SBAS DInSAR processing of sentinel-l data in a cloud computing environment," in *IGARSS*, IEEE. in Proc. IEEE Geoscience and Remote Sensing Symposium, 2018.

[19] M. Manunta, C. De Luca, I. Zinno, F. Casu, M. Manzo, M. Bonano, A. Fusco, A. Pepe, G. Onorato, P. Berardino *et al.*, "The parallel SBAS approach for sentinel-1 interferometric wide swath deformation time-series generation: Algorithm description and products quality assessment," *IEEE Transactions on Geoscience and Remote Sensing*, vol. 57, no. 9, pp. 6259–6281, 2019.

[20] N. Adam, F. R. Gonzalez, A. Parizzi, and R. Brcic, "Wide area Persistent Scatterer Interferometry: Current developments, algorithms and examples." IEEE, Jul. 2013, pp. 1857–1860.

[21] H. Ansari, F. Rodríguez-González, R. Brcic, and F. De Zan, "Evaluation of ensemble coherence as a measure for stochastic and systematic phase inconsistencies," in *Proc. IEEE Geoscience and Remote Sensing Symposium IGARSS*, Yokohama, Japan., 2019.

[22] F. R. Gonzalez, A. Parizzi, and R. Brcic, "Evaluating the impact of geodetic corrections on interferometric deformation measurements," in *Proc. 12th European Conference on Synthetic Aperture Radar (EUSAR)*, 2018.

[23] F. De Zan, A. Parizzi, F. R. Gonzalez, H. Ansari, G. Gomba, R. Brcic, and M. Eineder, "InSAR error budget for large scale deformation," in *Proc. IEEE International Geoscience and Remote Sensing Symposium IGARSS*, 2019.

[24] A. Parizzi, X. Cong, and M. Eineder, "First Results from Multifrequency Interferometry-A comparison of different decorrelation time constants at L, C, and X Band," *In Proc. Fringe Workshop*, 2009.

[25] P. Agram, R. Jolivet, and M. Simons, "Generic InSAR analysis toolbox (GIAnT)," *User Guide, ed*, 2012.

[26] Z. Li, T. Wright, A. Hooper, P. Crippa, P. Gonzalez, R. Walters, J. Elliott, S. Ebmeier, E. Hatton, and B. Parsons, "Towards insar everywhere, all the time, with sentinel-1." *International Archives of the Photogrammetry, Remote Sensing & Spatial Information Sciences*, vol. 41, 2016.

[27] H. Ansari, F. De Zan, and R. Bamler, "Sequential Estimator: Toward Efficient InSAR Time Series Analysis," *IEEE Transactions on Geoscience and Remote Sensing*, vol. 55, no. 10, pp. 5637–5652, Oct. 2017.

[28] H. Ansari, *Efficient High-Precision Time Series Analysis for Synthetic Aperture Radar Interferometry*. German Aerospace Center (DLR), ISSN: 1434-8454, 2019.

[29] H. Ansari, F. De Zan, and R. Bamler, "Distributed scatterer interferometry tailored to the analysis of Big InSAR Data," in *Proc. 12th European Conference on Synthetic Aperture Radar EUSAR*, Aachen, Germany., 2018.